that are different from Middle East. Although changes in human population density, climate conditions, and social factors may contribute to the spread of MERS-CoVs in other regions, the prevention of transmission at the animal/human interface is likely to be the most efficient measure to contain the threat from this virus.

REFERENCES AND NOTES

1. A. M. Zaki, S. van Boheemen, T. M. Bestebroer, A. D. Osterhaus, R. A. Fouchier, *N. Engl. J. Med.* **367**, 1814–1820 (2012).
2. A. Bermingham *et al.*, *Euro Surveill.* **17**, 20290 (2012).
3. World Health Organization, *Middle East Respiratory Syndrome Coronavirus (MERS-CoV)* (2015); www.who.int/emergencies/mers-cov/en/.
4. C. B. E. M. Reusken *et al.*, *Lancet Infect. Dis.* **13**, 859–866 (2013).
5. A. N. Alagaili *et al.*, *MBio* **5**, e00884-14 (2014).
6. E. I. Azhar *et al.*, *N. Engl. J. Med.* **370**, 2499–2505 (2014).
7. M. G. Hemida *et al.*, *Euro Surveill.* **18**, 20659 (2013).
8. B. Meyer *et al.*, *Emerg. Infect. Dis.* **20**, 552–559 (2014).
9. B. L. Haagmans *et al.*, *Lancet Infect. Dis.* **14**, 140–145 (2014).
10. U. Wernery *et al.*, *Emerg. Infect. Dis.* **21**, 1019–1022 (2015).
11. A. I. Khalafalla *et al.*, *Emerg. Infect. Dis.* **21**, 1153–1158 (2015).
12. D. R. Adney *et al.*, *Emerg. Infect. Dis.* **20**, 1999–2005 (2014).
13. M. A. Müller *et al.*, *Lancet Infect. Dis.* **15**, 559–564 (2015).
14. R. A. Perera *et al.*, *Euro Surveill.* **18**, 20574 (2013).
15. Materials and methods are available as supplementary materials on *Science* Online.
16. E. A. Farag *et al.*, *Infect. Ecol. Epidemiol.* **5**, 28305 (2015).
17. V. M. Corman *et al.*, *Emerg. Infect. Dis.* **20**, 1319–1322 (2014).
18. P. C. Woo *et al.*, *Emerg. Infect. Dis.* **20**, 560–572 (2014).
19. B. M. Crossley, R. E. Mock, S. A. Callison, S. K. Hietala, *Viruses* **4**, 3689–3700 (2012).
20. B. M. Crossley *et al.*, *J. Vet. Diagn. Invest.* **22**, 94–97 (2010).
21. G. Dudas, A. Rambaut, http://biorxiv.org/content/early/2015/06/12/020834 (2015).
22. V. M. Corman *et al.*, *J. Virol.* **88**, 11297–11303 (2014).
23. Q. Xie *et al.*, *Sci. China Life Sci.* **58**, 818–820 (2015).
24. Y. J. Kim *et al.*, *Genome Announc.* **3**, e00787–e15 (2015).
25. R. J. de Groot *et al.*, *J. Virol.* **87**, 7790–7792 (2013).

ACKNOWLEDGMENTS

We thank C.-H. Yip, C.-L. Cheung, Y. Chai, C. Ma, T. Gan, Z. Jin, Z. Ou, P. Huang, J. Zhou, and G. Yu for technical assistance and P. Kellam, A. Bin Saeed, M. Cotten, M. A. Barry, and A. M. Somily for making sequences available before their formal publication. This study was supported by the Deanship of Scientific Research (DSR 46-130-35-HiCi) of King Abdulaziz University; the Vice President for Educational Affairs A. O. Alyoubi under the umbrella of the Development Committee of Basic Sciences at King Abdulaziz University; the Shenzhen Peacock Plan High-End Talents Program (award KQTD201203); and the Li Ka Shing Foundation and Theme-based Research Scheme (award T11-705/14-N). E.C.H. is supported by an Australia Fellowship from the National Health and Medical Research Council of Australia (award AF30). All authors declare no competing financial interests. The sequences generated by this study were deposited in GenBank under accession numbers KT368824 to KT368916; additional data can be found in the supplementary materials.

SUPPLEMENTARY MATERIALS

www.sciencemag.org/content/351/6268/81/suppl/DC1
Materials and Methods
Figs. S1 to S5
Tables S1 and S2
References (*26*–*47*)

24 June 2015; accepted 12 November 2015
Published online 17 December 2015
10.1126/science.aac8608

GENOME EDITING

Rationally engineered Cas9 nucleases with improved specificity

Ian M. Slaymaker,[1,2,3,4]* Linyi Gao,[1,4]* Bernd Zetsche,[1,2,3,4] David A. Scott,[1,2,3,4] Winston X. Yan,[1,5,6] Feng Zhang[1,2,3,4]†

The RNA-guided endonuclease Cas9 is a versatile genome-editing tool with a broad range of applications from therapeutics to functional annotation of genes. Cas9 creates double-strand breaks (DSBs) at targeted genomic loci complementary to a short RNA guide. However, Cas9 can cleave off-target sites that are not fully complementary to the guide, which poses a major challenge for genome editing. Here, we use structure-guided protein engineering to improve the specificity of *Streptococcus pyogenes* Cas9 (SpCas9). Using targeted deep sequencing and unbiased whole-genome off-target analysis to assess Cas9-mediated DNA cleavage in human cells, we demonstrate that "enhanced specificity" SpCas9 (eSpCas9) variants reduce off-target effects and maintain robust on-target cleavage. Thus, eSpCas9 could be broadly useful for genome-editing applications requiring a high level of specificity.

The RNA-guided endonuclease Cas9 from microbial clustered regularly interspaced short palindromic repeat (CRISPR)–Cas adaptive immune systems is a powerful tool for genome editing in eukaryotic cells (*1*, *2*). However, the nuclease activity of Cas9 can be triggered even when there is imperfect complementarity between the RNA guide sequence and an off-target genomic site, particularly if mismatches are distal to the protospacer adjacent motif (PAM), a short stretch of nucleotides required for target selection (*3*, *4*). These off-target effects pose a challenge for genome-editing applications. Here, we report the structure-guided engineering of *Streptococcus pyogenes* Cas9 (SpCas9) to improve its DNA targeting specificity.

Several strategies to enhance Cas9 specificity have been reported, including reducing the amount of active Cas9 in the cell (*3*, *5*, *6*), using Cas9 nickase mutants to create a pair of juxtaposed single-stranded DNA nicks (*7*, *8*), truncating the guide sequence at the 5′ end (*9*), and using a pair of catalytically inactive Cas9 nucleases, each fused to a FokI nuclease domain (*10*, *11*). Although each of these approaches reduces off-target mutagenesis, they have a number of limitations: Reducing the amount of Cas9 can decrease on-target cleavage efficiency, double nicking requires the concurrent delivery of two single-guide RNAs (sgRNAs), and truncated guides can increase indel formation at some off-target loci and reduce the number of target sites in the genome (*12*, *13*).

[1]Broad Institute of MIT and Harvard, Cambridge, MA 02142, USA. [2]McGovern Institute for Brain Research, Massachusetts Institute of Technology, Cambridge, MA 02139, USA. [3]Department of Brain and Cognitive Sciences, Massachusetts Institute of Technology, Cambridge, MA 02139, USA. [4]Department of Biological Engineering, Massachusetts Institute of Technology, Cambridge, MA 02139, USA. [5]Graduate Program in Biophysics, Harvard Medical School, Boston, MA 02115, USA. [6]Harvard-MIT Division of Health Sciences and Technology, Harvard Medical School, Boston, MA 02115, USA.
*These authors contributed equally to this work. †Corresponding author. E-mail: zhang@broadinstitute.org

Cas9-mediated DNA cleavage is dependent on DNA strand separation (*14*, *15*). Mismatches between the sgRNA and its DNA target in the first 8 to 12 PAM-proximal nucleotides can eliminate nuclease activity; however, this nuclease activity can be restored by introducing a DNA:DNA mismatch at that location (*3*, *16*–*19*). We hypothesized that nuclease activity is activated by strand separation and reasoned that by attenuating the helicase activity of Cas9, mismatches between the sgRNA and target DNA are less energetically favorable, resulting in reduced cleavage activity at off-target sites (fig. S1).

The crystal structure of SpCas9 in complex with guide RNA and target DNA (*14*, *15*) provides a basis to improve specificity through rational engineering. The structure reveals a positively charged groove, positioned between the HNH, RuvC, and PAM-interacting domains in SpCas9, that is likely to be involved in stabilizing the nontarget strand of the target DNA (Fig. 1, A and B, and fig. S2). We hypothesized that neutralization of positively charged residues within this nontarget strand groove (nt-groove) could weaken nontarget strand binding and encourage rehybridization between the target and nontarget DNA strands, thereby requiring more stringent Watson-Crick base pairing between the RNA guide and the target DNA strand.

To test this hypothesis, we generated SpCas9 mutants consisting of individual alanine substitutions at 31 positively charged residues within the nt-groove and assessed changes to genome-editing specificity (Fig. 2A; fig. S3, A and B; and fig. S4). Single amino acid mutants were tested for specificity by targeting them to the *EMX1*(1) target site in human embryonic kidney (HEK) cells using a previously validated guide sequence; indel formation was assessed at the on-target site and three known genomic off-target (OT) sites (*3*, *4*). Five of the 31 single amino acid mutants reduced activity at all three off-target sites by a factor of at least 10 compared with wild-type (WT) SpCas9 while maintaining on-target cleavage

efficiency, and six others improved specificity by a factor of 2 to 5. These mutants also exhibited improved specificity when tested on a second locus, *VEGFA*(1) (Fig. 2B).

Although some single amino acid mutants were more specific than WT SpCas9 when targeting *EMX1*(1) and *VEGFA*(1), off-target indels were still detectable (~0.5%) (Fig. 2B). To further improve specificity, we performed combinatorial mutagenesis using the top single amino acid mutants identified in the initial screen. Eight out of 34 combination mutants retained wild-type on-target activity and displayed undetectable off-target indel levels at *EMX1*(1) OT1, *VEGFA*(1) OT1, and *VEGFA*(1) OT2 (Fig. 2C and fig. S3, C and D).

To ensure that the observed decrease in off-target activity was not accompanied by reduced on-target activity, we measured on-target indel formation at 10 target sites in three genomic loci using the top 14 mutants (fig. S5) and ranked these based on a combination of preserved on-target activity and decreased off-target activity. We identified three mutants with both high efficiency (WT levels of on-target indel formation) and specificity SpCas9 (K855A), SpCas9 (K810A/K1003A/R1060A) [also referred to as eSpCas9 (1.0)], and SpCas9 (K848A/K1003A/R1060A) [also referred to as eSpCas9(1.1)]. These three variants were selected for further analysis.

We expanded this assay to assess whether SpCas9(K855A), eSpCas9(1.0), and eSpCas9(1.1) broadly retained efficient nuclease activity, measuring on-target indel generation at 24 target sites spanning 10 genomic loci (Fig. 3A). All three mutants generated similar indel levels as WT SpCas9 with the majority of target sites (Fig. 3B). Mutants were expressed equivalently or at higher levels than WT SpCas9 based on a Western blot (Fig. 3C),

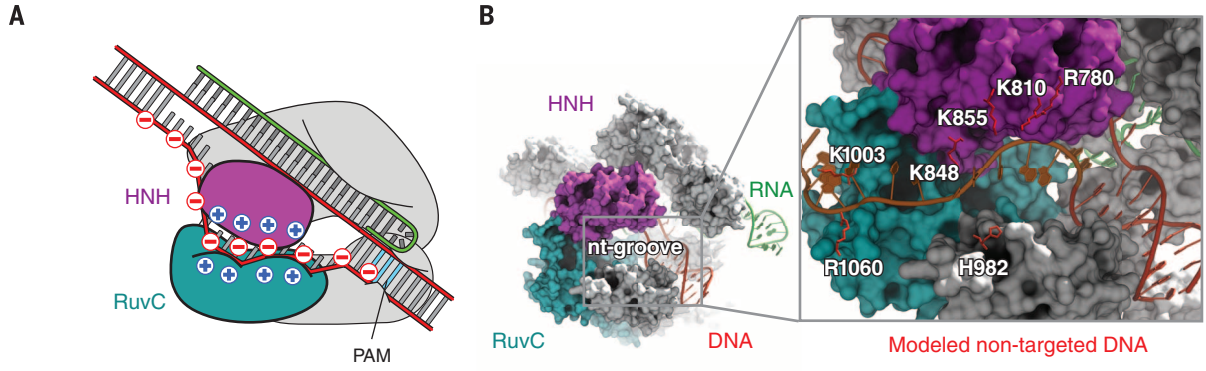

Fig. 1. Structure-guided mutagenesis improves specificity of SpCas9. (**A**) A model of Cas9 unwinding highlighting locations of charge on DNA and the nt-groove. The nt-groove between the RuvC (teal) and HNH (magenta) domains stabilizes DNA unwinding through nonspecific DNA interactions with the noncomplementary strand. RNA:cDNA and Cas9:ncDNA interactions drive DNA unwinding in competition against cDNA:ncDNA rehybridization. (**B**) A crystal structure of SpCas9 (Protein Data Bank ID 4UN3) showing the nt-groove situated between the HNH (magenta) and RuvC (teal) domains. The nontarget DNA strand (red) was manually modeled into the nt-groove (inset).

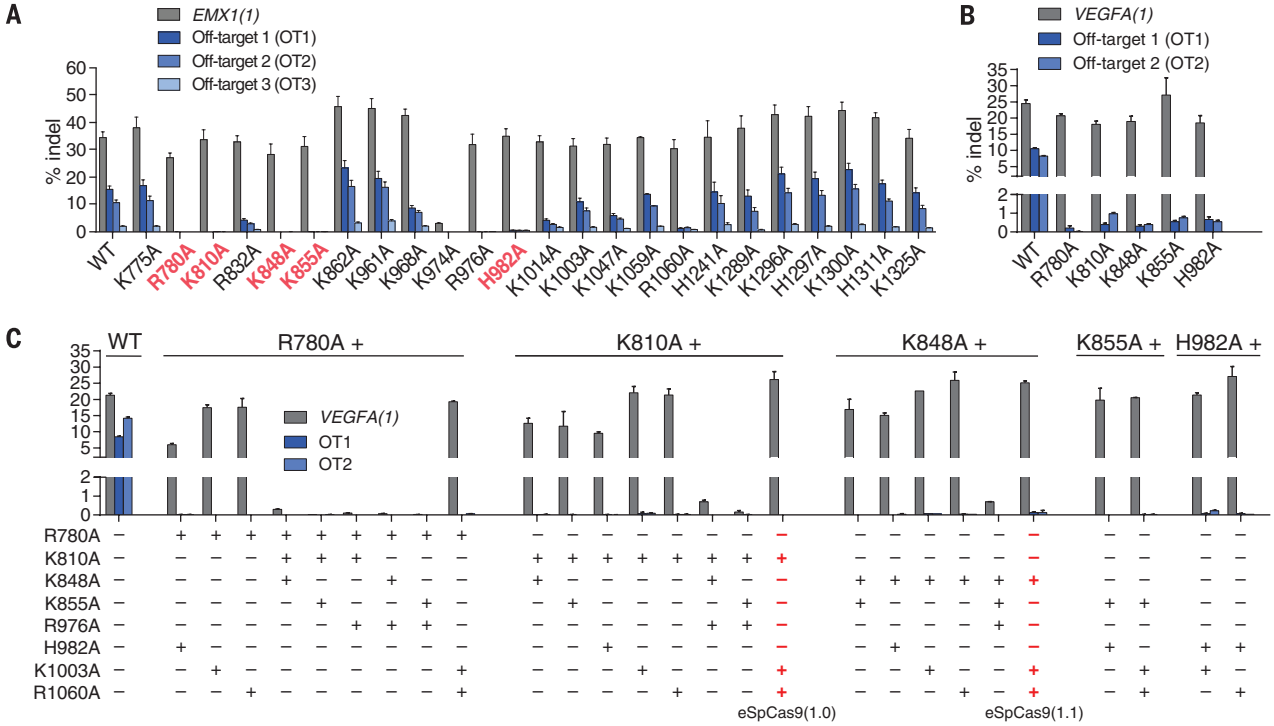

Fig. 2 Point mutations in Cas9 improve targeting specificity. (**A**) Screen of alanine single mutants for improvement in specificity. The top five specificity-conferring mutants are highlighted in red. (**B**) Assessment of top single mutants at additional off-target loci. (**C**) Combination mutants improve specificity compared with single mutants. eSpCas9(1.0) and eSpCas9(1.1) are highlighted in red.

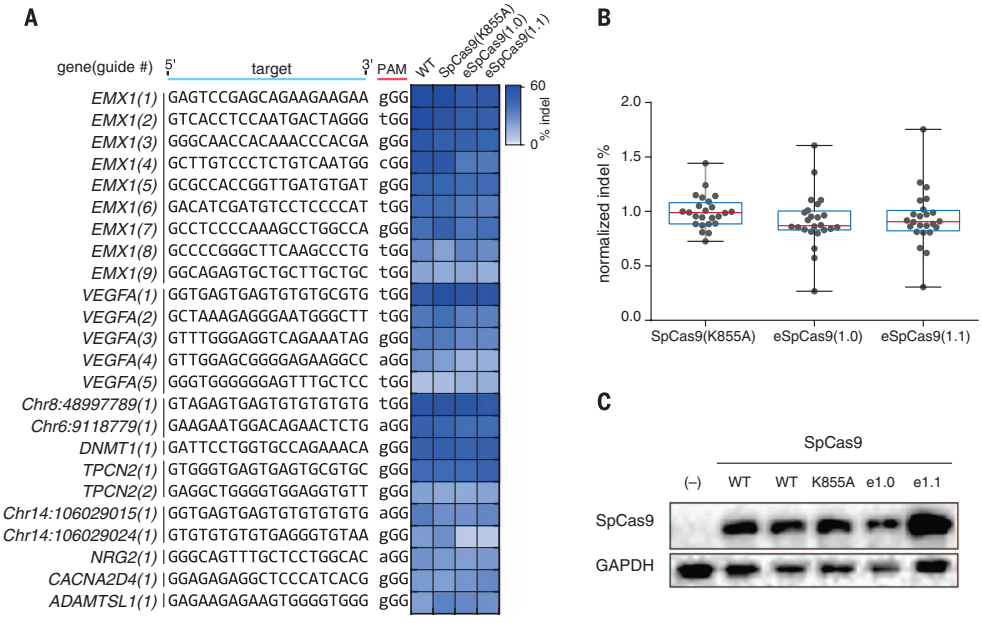

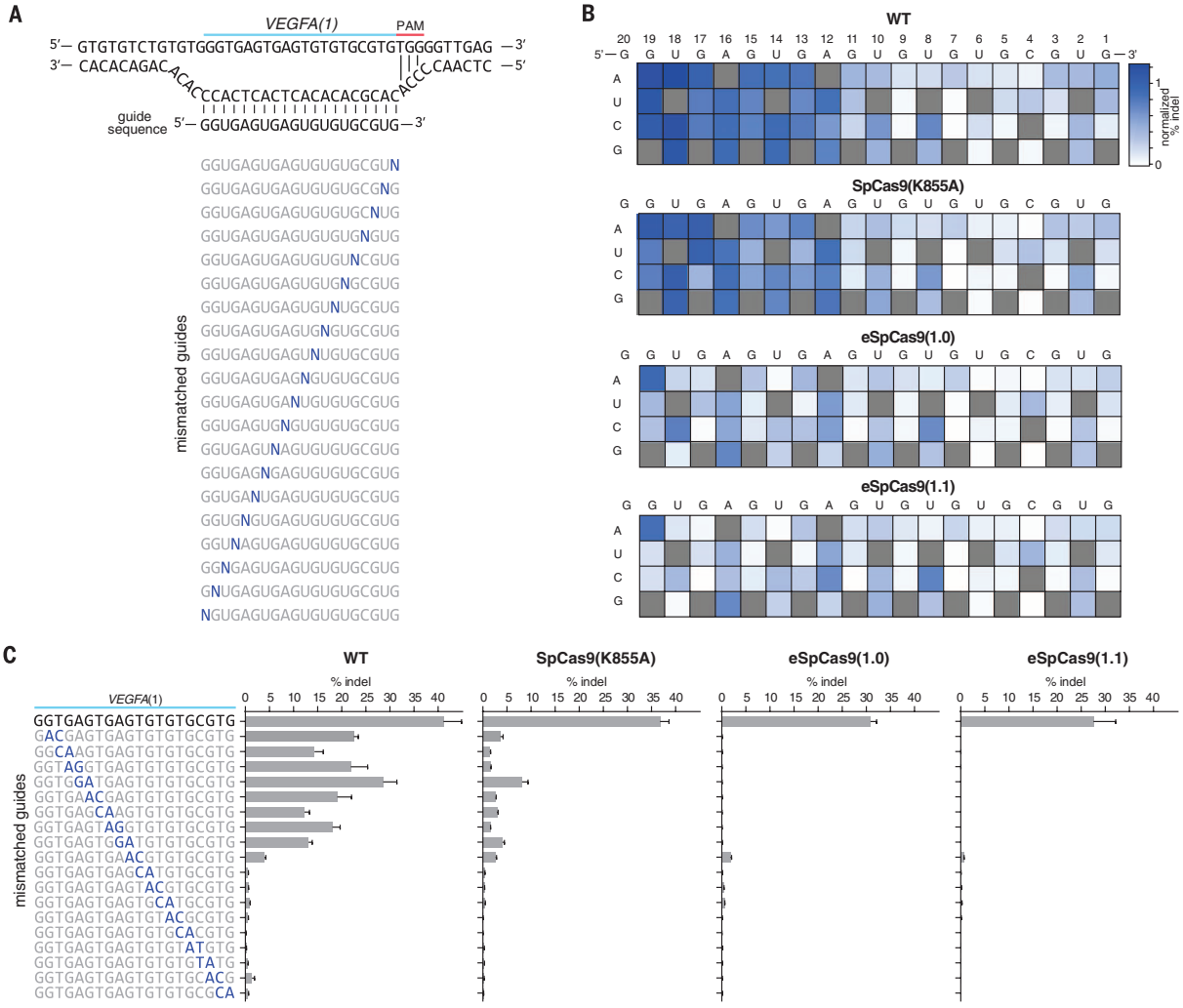

Fig. 3. SpCas9 mutants maintain on-target efficiency. (**A**) Assessment of mutants for efficient on-target cutting with 24 sgRNAs targeted to 10 genomic loci. (**B**) Box-and-whisker plot of normalized on-target indel formation for mutants. (**C**) Western blot of SpCas9 using antibody to SpCas9.

Fig. 4. SpCas9 mutants exhibited increased sensitivity to single- and double-base mismatches between the guide RNA and target DNA. (**A**) Schematic showing design of mismatched guide sequences against *VEGFA*(1). (**B**) Heat maps showing indel percentage of guide sequences with a single-base mismatch. (**C**) Indel formation with guide sequences containing consecutive transversion mismatches.

indicating that improvements in specificity were not due to decreased protein expression levels.

We compared the specificity of the three mutants to WT SpCas9 with truncated guide sequences [18 nucleotides for *EMX1*(1) and 17 nucleotides for *VEGFA*(1)], which have been shown to reduce off-target indel formation (*12*) (fig. S6). When using full-length (20 nucleotides) guides, all three mutants reduced cleavage at all off-target sites assessed compared with WT spCas9. Specifically, eSpCas9(1.0) and eSpCas9(1.1) with 20-nucleotide RNA guides eliminated cleavage at 22 out of 24 off-target sites (<0.2% indel). In contrast, WT SpCas9 with truncated guides eliminated 14 out of 24 sites but also increased off-target activity at five sites compared with WT SpCas9 with 20-nucleotide guides.

To further understand the tolerance SpCas9 (K855A), eSpCas9(1.0), and eSpCas9(1.1) for mismatched target sites, we systematically mutated the *VEGFA*(1) guide sequence to introduce single- and double-base mismatches at different positions (Fig. 4, A to C). Compared with WT SpCas9, all three mutants induced lower levels of indels with mismatched guides. Of note, eSpCas9(1.0) and eSpCas9(1.1) induced lower indel levels even with single-base mismatches located outside of the 7- to 12–base pair seed sequence. Given that we did not observe any difference between eSpCas9(1.0) and eSpCas9(1.1) in terms of specificity, we selected SpCas9(K855A) and eSpCas9(1.1) for further analysis based on on-target efficiency.

We assessed the genome-wide editing specificity of SpCas9(K855A) and eSpCas9(1.1) using BLESS (direct in situ breaks labeling, enrichment on streptavidin and next-generation sequencing) (*20*, *21*), which quantifies DNA double-stranded breaks (DSBs) across the genome (fig. S7A), for both the *EMX1*(1) and *VEGFA*(1) targets for both mutants and compared these results to WT SpCas9. We used a previously established computational pipeline for distinguishing Cas9-induced DSBs from background DSBs (*21*) (fig. S7B). Both SpCas9 (K855A) and eSpCas9(1.1) exhibited a genome-wide reduction in off-target cleavage and did not generate any new off-target sites (Fig. 5, A to D).

These findings also provide insight into the mechanism of Cas9 targeting and nuclease activity. We propose that off-target cutting occurs when the strength of Cas9 binding to the nontarget DNA strand exceeds forces of DNA rehybridization. Consistent with this model, mutations designed to weaken interactions between Cas9 and the noncomplementary DNA (ncDNA) strand led to a substantial improvement in specificity. The model also suggests that, conversely, specificity can be decreased by strengthening the interactions between Cas9 and the nontarget strand. Consistent with this hypothesis, we generated two mutants, S845K and L847R, each of which exhibited decreased specificity (fig. S8). Similar strategies described in this study can also be successfully applied to other Cas9 family proteins, such as *Staphylococcus aureus* Cas9 (SaCas9) (fig. S9), to engineer nucleases with improved specificity.

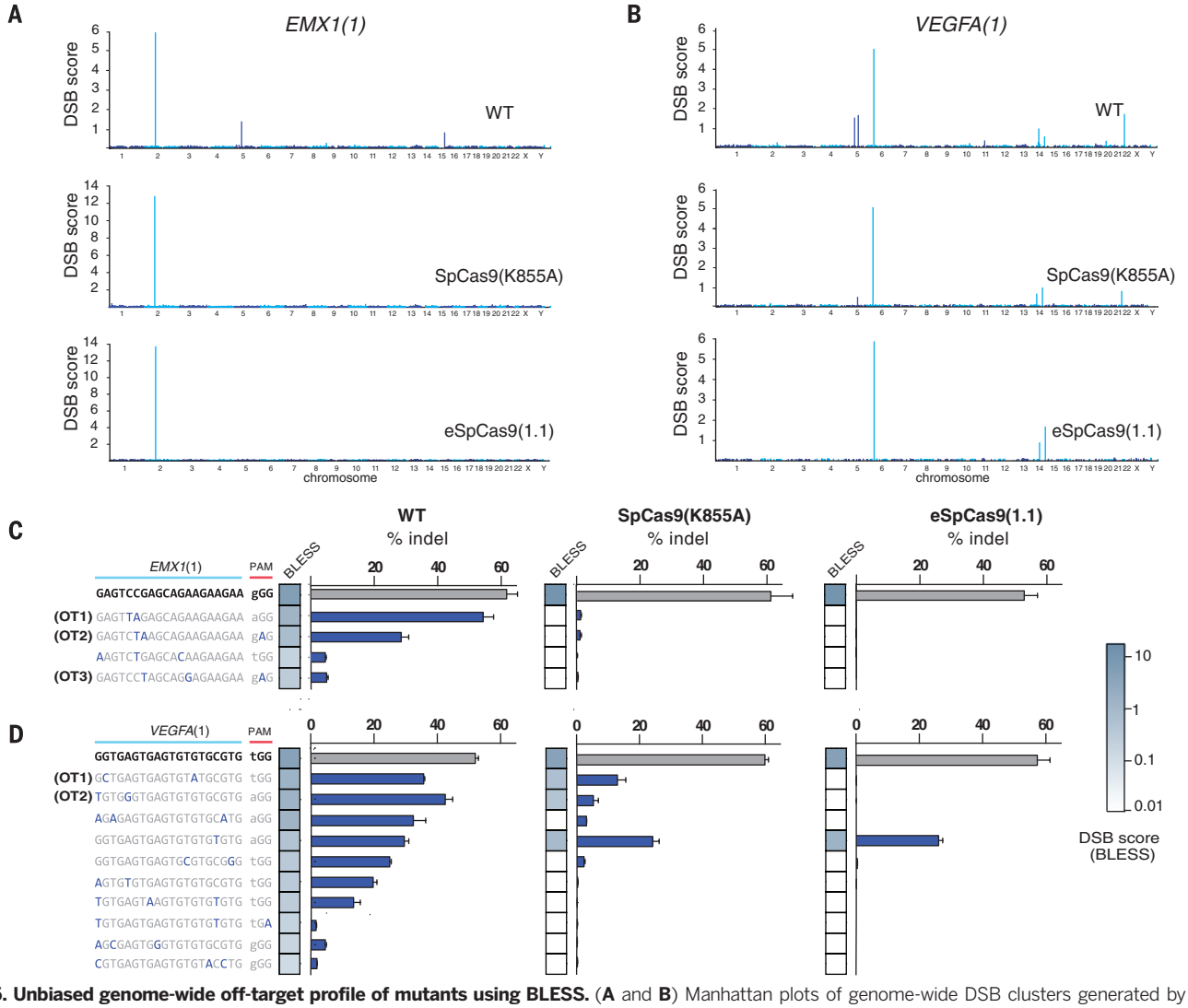

Fig. 5. Unbiased genome-wide off-target profile of mutants using BLESS. (**A** and **B**) Manhattan plots of genome-wide DSB clusters generated by each SpCas9 mutant using the *EMX1*(1) and *VEGFA*(1) targeting guides. (**C** and **D**) Targeted deep-sequencing validation of off-target sites identified in BLESS. Off-target sites are ordered by DSB score (blue heat map).

We have demonstrated through structure-guided design that neutralization of positive charges in the nt-groove can dramatically decrease off-target indel formation while preserving on-target activity. These data show that eSpCas9(1.1) can be used to increase the specificity of genome-editing applications. Future structure-guided interrogation of Cas9 binding and cleavage mechanism will likely enable further optimization of the CRISPR-Cas9 genome-editing toolbox.

REFERENCES AND NOTES

1. L. Cong *et al.*, *Science* **339**, 819–823 (2013).
2. P. Mali *et al.*, *Science* **339**, 823–826 (2013).
3. P. D. Hsu *et al.*, *Nat. Biotechnol.* **31**, 827–832 (2013).
4. Y. Fu *et al.*, *Nat. Biotechnol.* **31**, 822–826 (2013).
5. B. Zetsche, S. E. Volz, F. Zhang, *Nat. Biotechnol.* **33**, 139–142 (2015).
6. K. M. Davis, V. Pattanayak, D. B. Thompson, J. A. Zuris, D. R. Liu, *Nat. Chem. Biol.* **11**, 316–318 (2015).
7. F. A. Ran *et al.*, *Cell* **154**, 1380–1389 (2013).
8. P. Mali *et al.*, *Nat. Biotechnol.* **31**, 833–838 (2013).
9. Y. Fu, J. D. Sander, D. Reyon, V. M. Cascio, J. K. Joung, *Nat. Biotechnol.* **32**, 279–284 (2014).
10. S. Q. Tsai *et al.*, *Nat. Biotechnol.* **32**, 569–576 (2014).
11. J. P. Guilinger, D. B. Thompson, D. R. Liu, *Nat. Biotechnol.* **32**, 577–582 (2014).
12. Y. Fu, J. D. Sander, D. Reyon, V. M. Cascio, J. K. Joung, *Nat. Biotechnol.* **32**, 279–284 (2014).
13. S. Q. Tsai *et al.*, *Nat. Biotechnol.* **33**, 187–197 (2015).
14. H. Nishimasu *et al.*, *Cell* **156**, 935–949 (2014).
15. C. Anders, O. Niewoehner, A. Duerst, M. Jinek, *Nature* **513**, 569–573 (2014).
16. E. Semenova *et al.*, *Proc. Natl. Acad. Sci. U.S.A.* **108**, 10098–10103 (2011).
17. B. Wiedenheft *et al.*, *Proc. Natl. Acad. Sci. U.S.A.* **108**, 10092–10097 (2011).
18. W. Jiang, D. Bikard, D. Cox, F. Zhang, L. A. Marraffini, *Nat. Biotechnol.* **31**, 233–239 (2013).
19. S. H. Sternberg, S. Redding, M. Jinek, E. C. Greene, J. A. Doudna, *Nature* **507**, 62–67 (2014).
20. N. Crosetto *et al.*, *Nat. Methods* **10**, 361–365 (2013).
21. F. A. Ran *et al.*, *Nature* **520**, 186–191 (2015).

ACKNOWLEDGMENTS

We thank J. Dahlman for helpful discussions and a critical review of the manuscript; F. A. Ran, R. J. Platt, and J. Joung for experimental assistance; and the entire Zhang laboratory for support and advice. I.S. is supported by the Simons Center for the Social Brain. W.X.Y. is supported by T32GM007753 from the National Institute of General Medical Sciences and a Paul and Daisy Soros Fellowship. F.Z. is supported by the National Institutes of Health through NIMH (5DP1-MH100706 and 1R01MH110049) and NIDDK (5R01DK097768-03), a Waterman Award from the National Science Foundation, the Keck, New York Stem Cell, Damon Runyon, Searle Scholars, Merkin, and Vallee Foundations, and B. Metcalfe. F.Z. is a New York Stem Cell Foundation Robertson Investigator. I.S., L.G., B.Z., and F.Z. are inventors on provisional patent application 62/181,453 applied for by the Broad Institute and MIT that covers the engineered CRISPR proteins described in this manuscript. Plasmid DNA encoding eSpCas9(1.0) and eSpCas9(1.1) are available from Addgene under a Universal Biological Material Transfer Agreement with the Broad Institute and MIT. F.Z. is a founder and scientific advisor for Editas Medicine and a scientific advisor for Horizon Discovery. Further information about the protocols, plasmids, and reagents can be found at the Zhang laboratory website (www.genome-engineering.org).

SUPPLEMENTARY MATERIALS

www.sciencemag.org/content/351/6268/84/suppl/DC1
Materials and Methods
Figs. S1 to S12
Tables S1 to S3
Supplementary DNA Sequences
References

24 September 2015; accepted 18 November 2015
Published online 1 December 2015
10.1126/science.aad5227

PROTEIN TRANSLOCATION

Structure of the Sec61 channel opened by a signal sequence

Rebecca M. Voorhees and Ramanujan S. Hegde*

Secreted and integral membrane proteins compose up to one-third of the biological proteome. These proteins contain hydrophobic signals that direct their translocation across or insertion into the lipid bilayer by the Sec61 protein–conducting channel. The molecular basis of how hydrophobic signals within a nascent polypeptide trigger channel opening is not understood. Here, we used cryo–electron microscopy to determine the structure of an active Sec61 channel that has been opened by a signal sequence. The signal supplants helix 2 of Sec61α, which triggers a rotation that opens the central pore both axially across the membrane and laterally toward the lipid bilayer. Comparisons with structures of Sec61 in other states suggest a pathway for how hydrophobic signals engage the channel to gain access to the lipid bilayer.

The universally conserved Sec complex forms a gated protein translocation channel at the eukaryotic endoplasmic reticulum (ER) and bacterial plasma membrane (*1*). The central component of this channel, SecY in bacteria and Sec61α in eukaryotes, contains 10 transmembrane (TM) helices arranged around a central pore (*2*). Two single-TM subunits in eukaryotes, Sec61β and Sec61γ, are peripheral to Sec61α. The central pore in the inactive Sec complex is occluded by a short "plug" helix that must be displaced to allow translocation. The interface where TM helices 2 and 3 contact helices 7 and 8 defines a "lateral gate" for membrane access of polypeptides (*1–3*).

Crystal structures of the Sec complex (*2*, *4–6*) lack a translocating polypeptide and likely represent a range of inactive states. Depending on crystal contacts or translocation partners, the lateral gate and plug are in various states of opening and displacement. However, the biological relevance of these channel conformations has been difficult to interpret without a well-resolved and matched active structure. Previous structures of translocation or insertion intermediates of the ribosome-Sec complex determined by cryo–electron microscopy (cryo-EM) were of moderate resolution (*7–9*), contained heterogeneous substrates (*9*), required artificial stabilization (*8*), or were at an uncertain stage of insertion (*7*). Although these earlier structures provided the first views of substrate-induced structural changes consistent with lateral gate opening, the data could not clearly resolve individual Sec61 TM helices or the nature of their interactions with the signal. Thus, a molecular understanding of how substrates open the channel for translocation or insertion is incomplete.

We devised a strategy to tag and purify the canine ribosome-Sec61 complex engaged by the first 86 residues of the secretory protein preprolactin (fig. S1). Translocation, protease-protection, and photo–cross-linking experiments verified that, like the well-characterized native 86-residue intermediate (*10–15*), our tagged complex represents a functional translocation intermediate engaged by Sec61 (figs. S2 to S4). The nascent polypeptide remains engaged with Sec61 during and after purification (fig. S4), which makes it suitable for structure determination by single-particle cryo-EM.

The structure of this engaged ribosome-Sec61 complex was reconstructed from 101,339 particles to an overall resolution of 3.6 Å (figs. S5 and S6 and table S1). The local resolution of the Sec61 channel ranged from ~ 3.5 Å near the ribosome to ~7.0 Å at the lumenal loops. Most TM helices were at ~4.5 to 5.5 Å resolution (fig. S6), which revealed clear helical pitch and many bulky side chains in sharpened maps (fig. S7). All 12 TM helices of the Sec61 complex could be unambiguously assigned, leaving a single helix we ascribed to the signal sequence (Fig. 1, A and B, and fig. S8). Density visible throughout the ribosomal exit tunnel and in parts of the Sec61 channel (Fig. 1C) suggests a looped configuration for the nascent chain, consistent with earlier cross-linking studies (*11*).

The well-resolved structure of a biochemically validated early translocation intermediate permitted detailed comparisons with other Sec61 states to gain insights into the conformational changes accompanying channel opening. A previous cryo-EM structure of the porcine ribosome-Sec61 complex lacking a nascent polypeptide (*9*) represents a "primed" state preceding nascent chain insertion. Relative to this primed structure, the engaged channel is open laterally toward the lipid bilayer and axially across the membrane (Fig. 2). The ribosome-Sec61 interaction remains fixed, with only minor movements of the associated Sec61γ and TM helices 6, 7, 8, and 9 of Sec61α. The other seven TM helices of the Sec61 complex rotate as a rigid body by ~22° (Fig. 2A and movies S1 and S2), which creates space between helices 2 and 7 for intercalation of the signal peptide (Fig. 2B). Notably, cryo-tomography

MRC Laboratory of Molecular Biology, Medical Research Council, Francis Crick Avenue, Cambridge CB2 0QH, UK.
***Corresponding author. E-mail: rhegde@mrc-lmb.cam.ac.uk**